

Dust Continuum Radiative Transfer Model at Near InfraRed for the coreshine clouds

*A Project Report Submitted in partial fulfillment of the degree
of*

Bachelor of Science
from
Department of Physics
Tezpur University
submitted by
Abhilash Biswas
(PHI21020)

Under the guidance of
Dr. Rupjyoti Gogoi

*Assistant Professor, Tezpur University
in collaboration with*

Dr. Shalima Puthiyaveeti

Assistant Professor, Manipal Center for Natural Sciences



**DEPARTMENT OF PHYSICS
TEZPUR UNIVERSITY
NAPAAM 784001, Tezpur, Assam India
10 MAY, 2024**

CERTIFICATE

This is to certify that the project work entitled "**Dust Continuum Radiative Transfer Model at Near InfraRed for the coreshine clouds**" submitted to the School of Sciences, Tezpur University in partial fulfillment of the award for the Degree of **Bachelor of Science (B.Sc.) in Physics** is a record of study carried out by "**Abhilash Biswas**" under my supervision and guidance.

**Dr. Rupjyoti Gogoi
Assistant Professor
Department of Physics**

Date:

Forwarded by:

Certificate of Approval

The report submitted by **Abhilash Biswas (PHI21020)** is hereby approved as a creditable study carried out and presented in a manner satisfactory to warrant its acceptance as a prerequisite to the degree for which it has been submitted. It is understood that by this approval the undersigned do not necessarily endorse or approved any statement made, opinion expressed or conclusion drawn therein but approve only for the purpose for which it is submitted.

Date:

Forwarded by:

Dr. Jugal Lahkar:
Project Co-ordinator
Department of Physics
Tezpur University

Declaration

I, **Abhilash Biswas**, registered as an undergraduate student, with roll no. **PHI21020** for the Bachelors of Science Programme under the Department of Physics of Tezpur University do hereby declare that I have completed the requirements as per mentioned by the university for project submission. I do hereby declare that the project submitted is the outcome of the independent study carried out by me and contains no plagiarism. This work has not been submitted by any other University or Body in quest of a degree, diploma or any other kind of academic award. I do hereby further declare that the text, diagrams or any other material taken from other sources (including but not limited to books, journals and web) have been acknowledged, referred and cited to the best of my knowledge and understanding.

Date:

Signature of Student

ACKNOWLEDGEMENTS

I would like to acknowledge Department of Physics Tezpur University for providing me this opportunity to work on this project as a partial fulfillment in completion of Bachelors of Science in Physics degree. I am extremely grateful to my supervisor, **Dr. Rupjyoti Gogoi, Department of Physics, Tezpur University** and my co-supervisor **Dr. Shalima Puthiyaveetti, Deparement of Physics, Manipal Centre for Natural Sciences** for their suggestions, guidance and constant support. Their immense knowledge and plentiful experience have encouraged us to learn many new topics in the field of AstroPhysics. I would also like to thank the various researchers from various parts of the world who have helped me in this research and without whom this report would not have seen the light of day. And last but not the least, I would like to thank my friends and family for their constant support and motivation.

Abstract

This project investigates the spectral intensities of the molecular clouds of Taurus-Perseus, L183, Cepheus, and Chameleon Region. The focus is on studying the scattering of light by interstellar dust particles at Near InfraRed and modeling radiative transfer and to compare the infrared scattering intensities of the dusts with coreshine observations. The RADMC-3D software package is utilized for astrophysical radiative transfer calculations, enabling accurate simulations of the interaction between radiation, dust, and gas. We plot the image, SEDs and Extinction curve of our proposed model and compare it with $3.6\mu\text{m}$ coreshine observations from the works of [12]. This research contributes to a better understanding of the interstellar medium and its impact on stellar radiation.

Contents

| | | |
|-------|---------------------------------------------------------------------|----|
| 1.1 | Coreshine | 2 |
| 1.2 | Coreshine Observation Data | 3 |
| 2.1 | Basic Structure and functionality of Radmc3d | 4 |
| 2.1.1 | Basic Data Flow | 4 |
| 2.1.2 | Radiative Process | 5 |
| 2.1.3 | Computations | 5 |
| 2.1.4 | Setting Up a Model | 5 |
| 2.2 | Input Files | 6 |
| 2.3 | Scattering Modes | 7 |
| 3.1 | Physics of Stars and Envelopes | 10 |
| 3.1.1 | Formation of Stars | 10 |
| 3.1.2 | Main Sequence | 11 |
| 3.1.3 | End of Main Sequence | 13 |
| 3.2 | Envelopes and Dust Disks | 15 |
| 3.3 | Temperatures and spectrum of stars | 16 |
| 3.4 | Radiative Transfer | 16 |
| 3.4.1 | Dust continuum Radiative Transfer | 17 |
| 3.4.2 | Thermal Monte Carlo Simulation | 18 |
| 3.4.3 | Bjorkman Wood Algorithm (2001) | 18 |
| 3.4.4 | How does the method work? | 19 |
| 3.5 | Modified Random Walk Method | 20 |
| 4.1 | Model Setup | 21 |
| 4.1.1 | One Star Model | 21 |
| 4.2 | Verifying the results | 28 |
| 5.1 | Coreshine Data | 29 |
| 5.2 | One Star system | 29 |
| 5.2.1 | For Isotropic Scattering | 29 |
| 5.3 | For Anisotropic Scattering | 30 |
| 5.3.1 | For Userdefined Crossection and Phase Function Scattering | 30 |
| 5.3.2 | Model Images | 31 |
| 5.4 | Post-processing and comparision with real-world observations | 33 |
| 6.1 | Future Work | 34 |

Chapter 1

Introduction

Interstellar medium refers to any material present between stars. It is classified into interstellar dust and interstellar gas. The density of the interstellar medium is very low nearly about 1 atom/cm³. It is very low as compared to the density of Earth's atmosphere which is nearly 10^{19} atoms/cm³. Interstellar gas is further classified into ionized H-II gas regions which are found near hot stars and the UV rays of the stars ionize the Hydrogen in these regions. Then we have the neutral hydrogen gas clouds that are not detected and can only be detected when a star passes through the cloud. Next there are the cool hydrogen gas regions that emit a 21cm Hydrogen emission and emits radio waves. Next we have the ultra hot interstellar gas that can have temperatures of millions of degrees and finally the molecular clouds that in which UV rays break down the molecules to bring about complex chemical reactions. The next type of interstellar medium is the interstellar dust which is what we are more concerned with. These dust do not emit any light but it can scatter and reflect light from nearby stars. Interstellar dust is a good agent for scattering and also causes interstellar reddening which is a phenomenon in which a star appears redder than it usually is because of scattering of light by the dust particles. Interstellar reddening is a different phenomenon from red-shift, which is the proportional frequency shifts of spectra without distortion. Reddening preferentially removes shorter wavelength photons from a radiated spectrum while leaving behind the longer wavelength photons (in the optical, light that is redder), leaving the spectroscopic lines unchanged. These dust particles are made of interstellar dust grains which can have a core either rich in Carbon(sooty) or rich in Silicate(sand-like). In interstellar clouds, they are covered with a mantle of ice made of methane, ammonia and water.

1.1 Coreshine

Understanding the properties of dust within molecular clouds is crucial for unraveling the mysteries of star formation and the evolution of interstellar environments. Dust grains play a pivotal role in the radiative processes occurring within these dense regions, affecting both the scattering and absorption of radiation across various wavelengths.

In recent years, observations at mid-infrared wavelengths have unveiled a fascinating phenomenon known as "coreshine," shedding light on the densest regions of molecular clouds. Coreshine, predominantly observed at 3.6 and 4.5 micrometers, arises from scattering processes that dominate over absorption, offering a unique window into the physical conditions and dust properties within these environments.

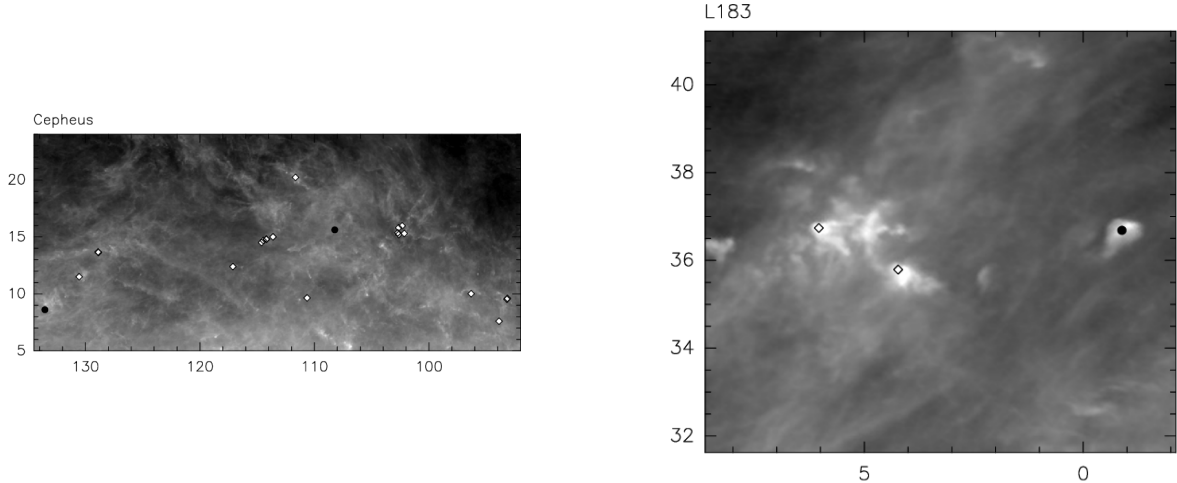
Building upon these advancements, our project aims to delve deeper into the intricacies of dust scattering and its implications for infrared emission within molecular clouds. Specifically, we seek to model the infrared scattering processes occurring within these clouds and compare our results with the coreshine intensities observed in the seminal work presented by [12].

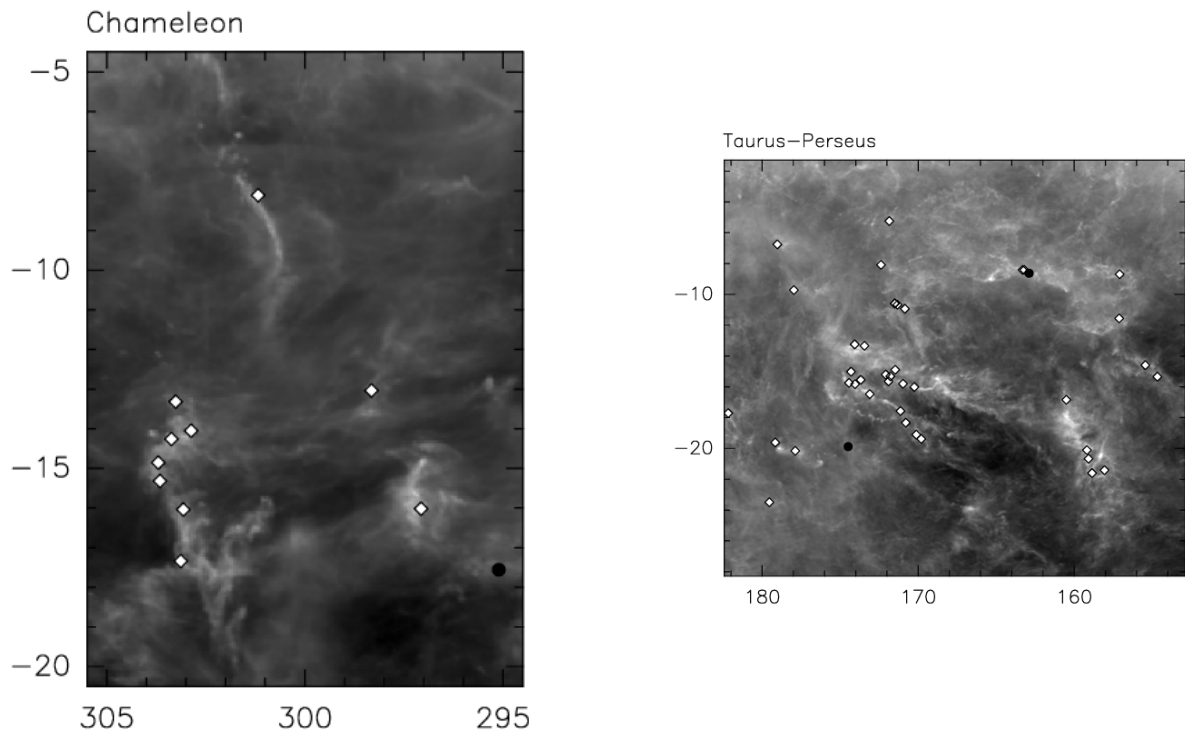
The methodology employed in our study involves the utilization of continuum radiative transfer techniques to simulate the propagation of infrared radiation through dusty environments. By integrating state-of-the-art dust models and environmental parameters derived from observations and theoretical considerations, we aim to construct a comprehensive framework capable of accurately reproducing the observed coreshine intensities. Central to our investigation is the comparison between the modeled infrared scattering properties and the coreshine observations reported in the literature. Through rigorous analysis and validation against observational data, we seek to elucidate the underlying dust properties, grain-size distributions, and physical conditions prevalent within molecular clouds.

Furthermore, our study underscores the importance of incorporating environmental parameters, such as interstellar radiation fields and the presence of embedded sources, in shaping the observed infrared emission characteristics. By carefully assessing these factors, we aim to provide valuable insights into the nature and evolution of dust within molecular clouds.

1.2 Coreshine Observation Data

- **NIR Data Collection:** Data in the Near-Infrared (NIR) spectrum were gathered using WIRCAM, a Wide Infrared Camera, with specific observations made in the J, H, and K bands. This instrument has a field of view of 20x20 arcminutes and a pixel size of 0.3 arcseconds. The data were collected for eight sources, including those situated in the Taurus region. This comprehensive coverage allowed for detailed examination of the selected targets and the surrounding areas.[12]
- **Coreshine Analysis with Spitzer:** To investigate coreshine, observations from the Spitzer Space Telescope were utilized. Specifically, data from the Infrared Array Camera (IRAC) were employed at wavelengths of 3.6, 4.5, 5.8, and 8 micrometers, supplemented by observations from the Warm mission. The analysis focused on molecular clouds, with regions of interest identified in Taurus, Perseus, Aquila, Aries, Cepheus, and Chameleon. These regions exhibited significant instances of coreshine phenomena. The table for the selected 72 coreshine dust are given.[12]





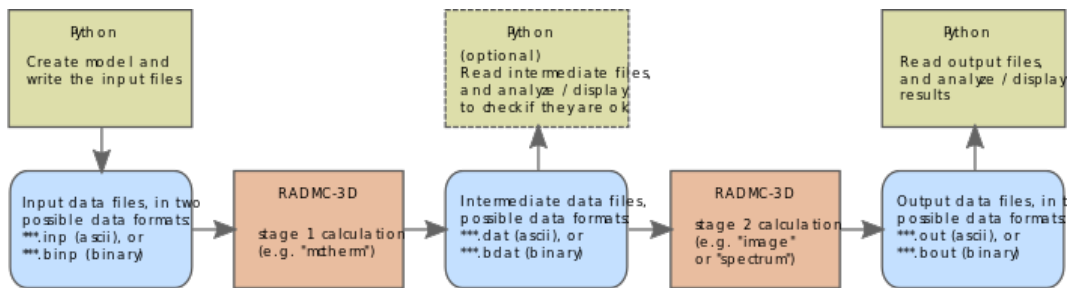
Chapter2

Introduction to Radmc3d

2.1 Basic Structure and functionality of Radmc3d

2.1.1 Basic Data Flow

The software package doesn't store any physical data on its own. It is completely dependent on the input files for its functioning. The input files have extensions .inp or .binp depending on whether the files are binary or ASCII files.



2.1.2 Radiative Process

Radmc3D is a powerful tool that is capable of performing the following radiative processes:

- Dust Thermal Emission and Absorption Spectra
- Dust Scattering
- Gas Molecular Size

2.1.3 Computations

Radmc3D is capable of performing the following computations:

- Compute the Dust Temperature using the radmc3d mctherm command.
- Compute Spectral Energy Distribution(SED) using the radmc3d.
- Compute an image using radmcIntroduction to Radmc3D3d image command.
- Compute the local radiation field inside the model using the radmc3d mcmono command.

2.1.4 Setting Up a Model

To set up a model in radmc3D, the user needs to perform the following steps:

- A user must specify the 3-D distribution of dust and/or gas in a coordinate system (cartesian or spherical) and a spatial grid.

- The average densities of dust and/or gas are specified in cells on the grid in a file called amr grid.inp.
- The locations and properties of one or more stars in the model are specified in the stars.inp file.
- To compute the appearance of the model in dust continuum, a user must write a file called dust density.inp to specify the density of dust in each cell and provide dust opacity tables in files called dustopac.inp and dustkappa silicate.inp.
- RADMC-3D requires a table of discrete wavelengths in the file wavelength micron.inp to perform its calculations on.
- RADMC-3D performs a Monte Carlo simulation to compute dust temperatures everywhere and writes this to the file dust temperature.dat.
- To make a spectral energy distribution or image, the user calls radmc3d sed or radmc3d image, respectively.
- RADMC-3D reads all its information from tables in various files, which can be generated using a little computer program in any programming language.

2.2 Input Files

In order to perform any of the dust radiative transfer simulations we must give radmc-3D, some input files. Some of them are listed below:

1. **Amr.inp:** This is the grid file
2. **Wavelength micron.inp:** The global wavelength file
3. **Stars.inp:** defines the locations and properties of stars
4. **Dust density.inp:** This file defines the spatial distribution of dust in the grid.

5. **Dustopac.inp:** a file containing general data about the different types of dust in the model. The number of dust species included in the model and their tag names are two of the key pieces of information provided here (see dustkappa XXX.inp below). One density distribution for each dust species must be present in the file dust density.inp, which must have exactly this amount of density distributions.
6. **dustkappa XXX.inp:** A file or files containing dust opacity, where XXX should actually be a tag name we provide, such as dustkappa silicate.inp. The dustopac.inp file contains a list of the labels.
7. **Camera wavelength micron.inp(optional):** Only when creating a spectrum at a specific range of wavelengths do we need to utilise this file; otherwise, radmc3d sed should be used.
8. **mcmono wavelength micron.inp(optional):** Only if we want to compute the radiation field inside the model by executing radmc3d mcmono (for example, for photochemistry), do we require the file

2.3 Scattering Modes

From scattering mode=1 (the simplest) through scattering mode=5, RADMC-3D offers five levels of scattering treatment realism:

1. **No Scattering :** No scattering (scattering mode=0): Scattering is disregarded if the dustkappa XXX.inp files lack a scattering opacity or if scattering is disabled by setting scattering mode max to 0 in the radmc3d.inp file. The dust particles are then believed to have no albedo.
2. **Isotropic Scattering :** Scattering is considered as isotropic scattering if either the dustkappa XXX.inp files lack information regarding the anisotropy of the scattering or anisotropic scattering is disabled by setting scattering mode max to 1 in the radmc3d.inp file. Be aware that this is only a rough estimate. For isotropic scattering(scattering mode=1), the scattering source function is given by:

$$\mathbf{j}_v^{\text{scat}} = \alpha_v^{\text{scat}} \frac{1}{4\pi} \int \mathbf{I}_v d\omega$$

3. **Anisotropic scattering using Henyey-Greenstein (scattering mode=2)** [14]: Anisotropic scattering is handled using the Henyey-Greenstein approximate formula if the dustkappa XXX.inp files contain the scattering opacity and the g parameter of anisotropy (the Henyey-Greenstein g parameter, which is equal, by definition, to $g = \cos\theta$, where θ is the scattering deflection angle). For scattering mode = 2, we have the Henyey-Greenstein function phase function defined as:

$$\phi(\mu) = \frac{(1 - g^2)}{(1 + g^2 - 2g\mu)^{\frac{3}{2}}}$$

where the value of the anisotropy parameter g is taken from the dust opacity file. We should note that for $g = 0$ we will get $\phi(\mu) = 1$ which is the phase function for isotropic scattering.

4. **Anisotropic scattering using tabulated phase function (scattering mode=3):** We must describe the dust opacities using dustkap-scatmat XXX.inp files rather than the less complex dustkappa XXX.inp files in order to tackle scattering using a tabulated phase function. Additionally, scattering mode max needs to be set to 3 or above. If we have scattering mode=3 then the phase function is tabulated by us. We have to provide the tabulated phase function as the Z 11 () scattering matrix element or a tabulated set of values, and this is done in a file dustkapscatmat xxx.inp. The relation between Z 11 () and $\phi(\mu)$ is:

$$\phi(\mu) = \phi(\cos\theta) = \frac{4\pi}{k_{\text{scat}}} \mathbf{Z}_{11}(\theta) \mathbf{r}$$

5. **Anisotropic scattering with polarization for last scattering (scattering mode = 4):** We must supply the entire dust opacity and scattering matrix using the dustkapscatmat XXX.inp files rather than the more straightforward dustkappa XXX.inp files in order to treat scattering off randomly oriented particles with the full polarisation. If scattering mode=4, the full polarisation is only applied

during the final scattering before the light reaches the observer (i.e., it is only taken into account when computing the scattering source function that is used to create the images, but it is not taken into account when simulating the movement of the photons in a Monte Carlo simulation). If we have scattering mode=4 then the scattering in the Monte Carlo code is done according to the tabulated (μ)mode mentioned above, but for computing the scattering source function the full polarized scattering matrix is used.

6. **Anisotropic scattering with polarization, full treatment (scattering mode=5):** Setting scattering mode max to 5 and utilising the more complex dustkapscatmat XXX.inp files to provide the full dust opacity and scattering matrix are required for the complete treatment of polarised scattering off randomly oriented particles. If we have scattering mode=5 then the scattering phase function is not only dependent on μ but also on the other angle. And it depends on the polarization state of the input radiation.

Chapter 3

Theoretical Background

3.1 Physics of Stars and Envelopes

Understanding the realistic parameters for stars is essential for assessing the validity of our models, as RADMC3D enables us to create configurations that may not correspond to actual stellar characteristics. Although the program permits us to generate stars with extreme features such as a radius 10 times that of the Sun and a temperature of 1 K, such configurations are not representative of real stars. Thus, it's crucial to be cognizant of the plausible traits of stars.

- M_{\odot} - Mass of the Sun = $1.9884 * 10^{30}$ kg
- R_{\odot} - Radius of the Sun = $6.96342 * 10^8$ m

Henceforth the index \odot always refers to the sun.

3.1.1 Formation of Stars

Stars typically form within denser regions of the interstellar medium, often within molecular clouds where hydrogen (H_2) constitutes approximately 70 % of the mass, accompanied by CO and helium. Heavier elements are typically found in dust particles at a rate of about 1%. Interstellar clouds typically have a density of 100 particles/cm³, a diameter of $9.5 * 10^{14} km$, a mass of up to $6 * 10^6 M_{\odot}$, and an average temperature of 10 K. H_2 , lacking a dipole moment, cannot be observed between 10 and 20 K and is unsuitable for direct observation. However, CO, the second-most common gas in interstellar clouds, emits detectable radio waves, especially during rotational transitions known as quadruple transitions. The amount of CO can be used to estimate the amount of H_2 in the cloud, assuming a constant ratio of H_2 to CO molecules. Satellite observations in the far-infrared spectrum pro-

vide another method to estimate H abundance, as terrestrial observations are hindered by the Earth's atmosphere. Wavelength-dependent extinction observations offer a unique technique, where dust clouds cause stars to appear reddish due to scattering, allowing for mass calculations assuming a constant H to dust ratio. Gravitational collapse within interstellar clouds is primarily driven by gravitational pulls toward high-density cores and gas pressure. Once a cloud reaches the Bonnor-Ebert mass (M_{BE}), gravitational forces overcome gas pressure, initiating collapse. As the collapse progresses, H dissipates into atomic hydrogen (H), leading to the formation of a protostar. The formation process is further complicated by the conservation of angular momentum, resulting in the gas forming a disk due to rotational forces and gravitational attraction toward the center. Magnetic fields within the cloud can also influence star formation significantly. For a more in-depth understanding, advanced works like "Evolution of Stars and Stellar Populations" by Maurizio Salaris and Santi Cassisis are recommended, which delve into topics such as the Main Sequence phase in a star's evolution.

3.1.2 Main Sequence

Stars provide information through electromagnetic radiation, which includes their luminosity (total energy emitted per unit time) and temperature at the photosphere. Since stars are considered almost blackbodies, their temperature is typically represented by the effective temperature, denoted as T_{eff} . While determining a star's temperature requires analyzing its spectrum, the luminosity can be measured at a given distance. However, calculating the effective temperature and luminosity of a star is a time-consuming process. As a result, two alternative quantities are commonly used to characterize stars. The absolute magnitude M v in the visual band, specifically the V band, describes the intrinsic flux (energy in the visual range per unit wavelength, area, and time). When the distance to an object increases, the flux decreases accordingly. To determine the absolute brightness of a star, a standard distance of 10 parsecs (pc) is generally assumed. [8]

$$M_v = \frac{-2.5 \log_{10}(F_v(10pc))}{F_0(10pc)}$$

It is possible to apply this formula to any distance and any wavelength. Given that the flux diminishes with the apparent magnitude of an object by $r - 2$, the magnitude of an object as seen from Earth can be expressed as:

$$m_\lambda = M_\lambda + 5 \log \frac{r}{1 - pc}$$

Higher mass stars typically have greater luminosity. The following equations provide the link between a star's brightness and mass:

$$\frac{L}{L_\odot} = \left(\frac{M}{M_\odot}\right)^a$$

where M is the star's mass and L is the star's luminosity. The value of the exponent a falls between 1 and 6. If the star's mass is between 2 and 20 M_\odot , the answer for stars on the main sequence is 3.5. We should keep in mind that extremely massive stars frequently exceed the $20 M_\odot$ limit and must be calculated accordingly. Instead of the effective temperature (T_{eff}), the color of a star can be used as an alternative quantity. Assuming that a star can be reasonably modeled as a blackbody, its color is indicative of its temperature. The ratio of the flux in the visual band (F V) to the flux in the blue band (F B), known as (B-V), is often employed for this purpose. This approach assumes that there are no interposing substances such as dust or gas between the observer and the star. Spectral types, which are determined by the relative strengths of specific lines in a star's spectrum, are commonly used as well. These spectral types, denoted by letters O, B, A, F, G, K, M (in order of decreasing temperature), have historical origins and are not directly based on T_{eff} . However, they exhibit a strong correlation with the actual temperatures of the stars. It's worth noting that spectral types are defined by specific absorption and emission lines within certain frequencies (e.g., Class O is defined by the ratio of N IV 4058 to N III 4634), rather than by T_{eff} itself. The protostar's so-called pre-main sequence evolutionary track is the path it takes in the HRD when it becomes stars. The so-called Hayashi-track is the line where young stars with masses below $3 M_\odot$ basically 'fall down' in the HRD while stars with higher masses develop a fully radiative interior, which leads from the Hayashi to a pronounced Henyey-track, a bent track as seen in Figure 3.2. One theory for the accumulation of objects on the

Main Sequence is that stars require a long period of hydrostatic equilibrium in order to be stable. In order to maintain an equilibrium between gravity and gas pressure (and, for huge stars, radiation pressure), stars must have a specific mass and radius. The stellar radius and temperature are related through:

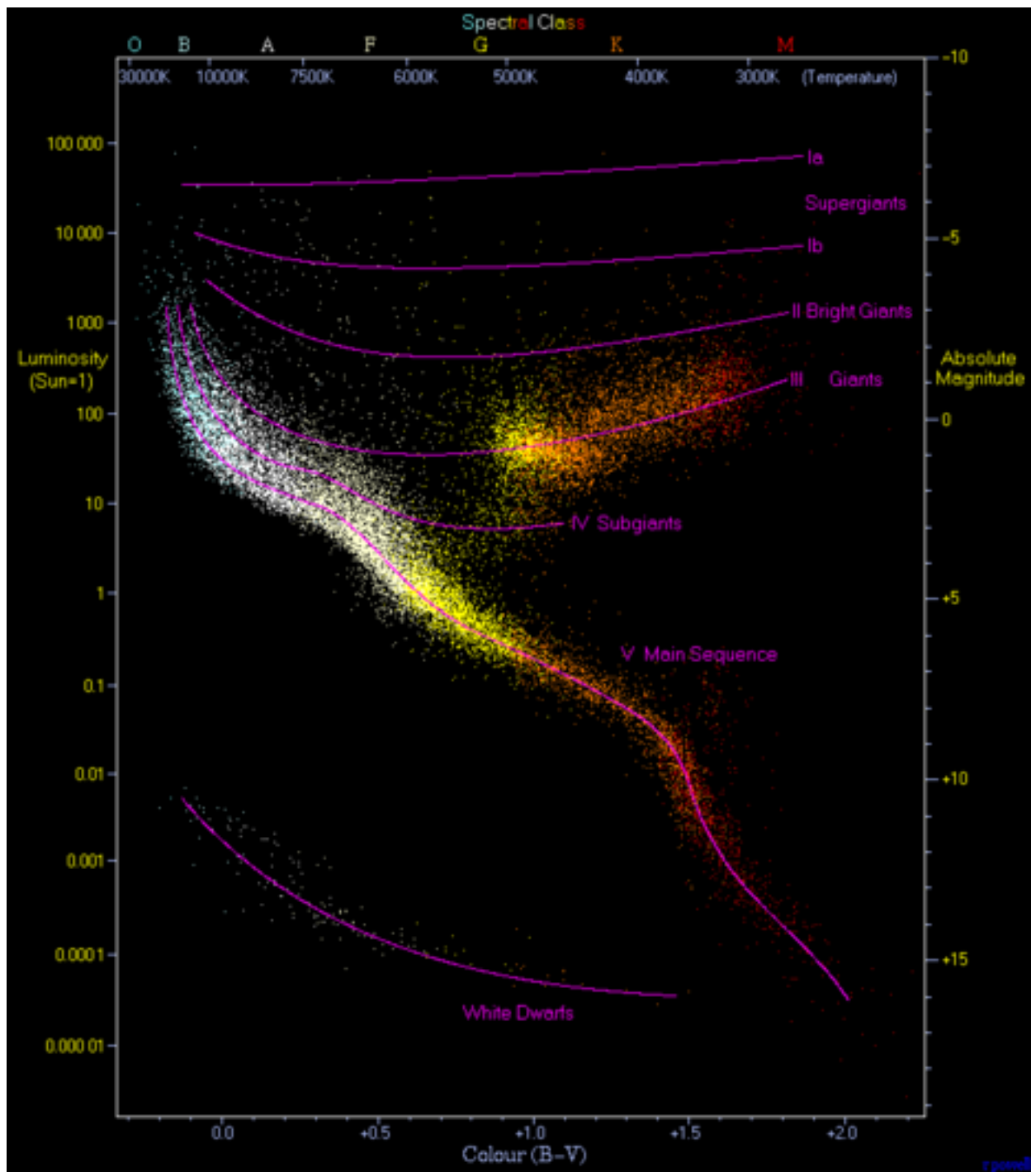
$$L_{star} = 4\pi(R_{star}^2\sigma_B(T_{eff})^4)$$

Luminosity (L) is directly related to effective temperature (T_{eff}) through the Stefan-Boltzmann constant (σ_B), establishing the main sequence as the predominant evolutionary stage for stars. Due to the instability or implausibility of intermediate stages, few stars exhibit characteristics of the giant- or main branch.

On the main sequence, there exists a discernible correlation between a star's mass and its hydrogen-burning rate, resulting in shorter lifespans for high-mass stars and significantly longer lifespans for low-mass ones. For instance, stars with a mass of $60 M_\odot$ have lifespans of roughly $3.4 * 10^6$ years, whereas those with a mass of $1 M_\odot$ can persist for approximately $1 * 10^{10}$ years. As stars age, they ascend the Hertzsprung-Russell Diagram due to helium accumulation in their cores, leading to contraction and subsequent re-ignition, initiating fusion in outer hydrogen layers, thereby increasing radius and luminosity over time. Although stars predominantly fuse hydrogen to helium in their cores, they will inevitably deplete their fuel, marking the conclusion of the main sequence. For more comprehensive insights into this intricate subject, Steven W. Stahler and Francesco Palla's "The Formation of Stars" is recommended.

3.1.3 End of Main Sequence

As hydrogen is consumed to produce helium, a shell of hydrogen-burning material surrounds the helium-rich core. Continuously supplying helium to the core, this shell eventually collapses under gravitational and pressure forces from the overlying layers. The star rapidly transitions to the so-called giant branch, situated in the upper right corner of the HRD, due to envelope expansion induced by shell burning, enhancing brightness while lowering temperature. Eventually, it progresses to the left on the HRD, reaching the horizontal branch, where core temperatures enable helium fusion. At this stage, distinguishing between three primary regimes is essential due to the vast range of star masses and their varied end-of-life



scenarios. Stars with masses between 75 Jupiter masses (M_J) and less than $0.4 M_{\odot}$ lack the mass for helium fusion, leading to white dwarf formation, stabilized by electron degeneracy pressure. Stars with masses from 0.4 to $2.3 M_{\odot}$, capable of helium burning, evolve into red giants before forming

white dwarfs if they fail to fuse heavier elements. Planetary nebulae form as outer layers are shed. Heavier stars (more than $2.3 M_{\odot}$) proceed to burn carbon and heavier elements, shedding outer layers to become supergiants or culminating in supernovae, which may leave behind neutron stars or black holes if their remaining mass is sufficient. Black holes, with masses exceeding about 3 solar masses, are detectable only through gravitational or accretion disc radiation due to their extreme density, preventing even light from escaping. Ultimately, remnants from deceased stars contribute to interstellar matter, crucial for new star formation, with supernovae serving as the primary source of elements beyond iron. While Radmc3d can model giant and dwarf stars to a degree, it's important to note its limitations, as the program isn't designed for simulating neutron stars or black holes.

3.2 Envelopes and Dust Disks

Given that radmc3d primarily models stars within envelopes and dust disks, it's imperative to delve into their formation process. A circumstellar envelope envelops the star during the collapse of a massive molecular cloud. As mass migrates from outer regions to the core, the star's rotational velocity escalates due to angular momentum conservation. Centripetal forces hinder direct infall of material near the rotational plane, while material closer to the axis experiences quicker descent. Denser equatorial material pulls adjacent material towards the axis, mitigating angular momentum effects via friction, initially forming a conical-shaped circumstellar envelope, which later evolves into circumstellar disks. A bipolar outflow, along the rotational axis, expels hot gas into space. For further insights on bipolar outflows, consult Adam Franks' "Bipolar outflows and the evolution of stars." While interstellar gas absorbs a limited wavelength range, dust particles exhibit broad absorption bands, crucial for cooling nascent stars. Portions of gas within the disk accrete, while the majority succumbs to radiation pressure, albeit less impactful on dust. This results in debris discs, potentially forming protoplanets or colliding with the star. During this phase, the dust-to-gas ratio fluctuates significantly, influenced by the star's gas and radiation pressure. Circumstellar discs endure for up to 10 million years, whereas bipolar outflows, or jets, are short-lived, especially for hotter, more massive stars due to heightened radiation pressure.

Young stellar objects are often associated with envelopes and discs, though older stars, like Mira variables, possess circumstellar envelopes, warranting consideration for models of evolved stars.

3.3 Temperatures and spectrum of stars

While the characteristics of stars on the main sequence have been discussed, it's essential to consider the temperatures of stars after they depart from this stage. For instance, white dwarfs may have surface temperatures as low as 3000 K, while massive stars, buoyed by their intense radiation pressure, can exhibit surface temperatures as high as 210,000 K, unveiling layers that burn at higher temperatures. Radmc3d can plot spectra, facilitating the alignment of models with observational data. Hence, describing the components of star spectra becomes crucial. Effective temperatures, derived from luminosity as discussed in the 'Main Sequence' section, can be compared with black body temperatures since stars can be reasonably approximated as black bodies. Depending on their metallicity and surrounding materials, stars manifest absorption and occasionally emission lines in their spectra, contributing to spectral classifications. Proto-stars and very young stellar objects often exhibit a second peak due to the emission of surrounding gas at lower temperatures, detectable through infrared wavelengths. It's important to acknowledge that gases may harbor additional energy sources such as rapid rotation or magnetic flux, which can influence the spectrum. Spectral analysis may sometimes be misleading, portraying stars as older than they are due to higher metallicities. Younger stars typically possess lower metallicities as they either haven't reached temperatures necessary for fusion beyond helium or haven't had sufficient time to accumulate the metallicity present in their outer shells. This discrepancy can arise, for instance, if the star formed in a planetary nebula with high metallicity.

3.4 Radiative Transfer

Radiative transfer describes the change of intensity and energy of radiation through absorption, scattering and emission. When modeling stars that are located in clouds of gas and dust it is of utmost importance to consider the influence of the matter on radiation. The radiative transfer equation

is given by :

$$\frac{dI_v}{ds} = j_v^{therm} + j_v^{scat} - (\alpha_v^{abs} + \alpha_v^{scat})I_v$$

where, j_v^{therm} is the thermal Source function , j_v^{scat} is the scattering source function , and, $(\alpha_v^{abs} + \alpha_v^{scat})$ are the extinction terms.

3.4.1 Dust continuum Radiative Transfer

The process of dust continuum radiative transfer involves the interaction of electromagnetic radiation with dust particles within a medium, such as interstellar or intergalactic space, wherein the radiation is either absorbed or scattered by the dust particles. This process plays a crucial role in comprehending the characteristics of the dust, as well as the radiation field and energy equilibrium within astrophysical settings. In astrophysical scenarios, dust grains are typically much smaller than the wavelength of the radiation they engage with, thereby allowing their interaction to be interpreted as the scattering or absorption of a continuum of wavelengths. The manner in which radiation interacts with dust grains is contingent upon various factors, including the size and composition of the dust grains, the temperature and density of the medium, and the intensity and spectrum of the radiation. The fundamental principles of dust continuum radiative transfer can be encapsulated within the equation of radiative transfer, which establishes a connection between the intensity of the radiation field and the absorption and scattering characteristics of the dust grains. In its simplest manifestation, this equation can be analytically solved for a homogeneous and isotropic medium with a uniform dust distribution. Nonetheless, in numerous astrophysical contexts, the medium exhibits complexity, and the distribution of dust is non-uniform, thereby significantly complicating the problem. To tackle these intricacies, numerical methodologies like Monte Carlo simulations or finite-difference methods are frequently employed. These techniques enable the computation of the effects of scattering and absorption across a broad spectrum of dust properties and environmental conditions, thereby furnishing insights into the physical mechanisms that oversee the formation and progression of dust within astrophysical settings.

3.4.2 Thermal Monte Carlo Simulation

The thermal Monte Carlo method serves as a computational tool for modeling physical systems operating at finite temperatures, especially beneficial for investigating systems featuring numerous interacting particles, such as gases, liquids, and solids. In this approach, the system is depicted as a collection of particles, with their positions and velocities evolving according to probabilistic rules derived from thermodynamic principles. The fundamental concept underlying the thermal Monte Carlo method involves sampling the system's configuration space through a series of random moves, each move being accepted or rejected based on its associated probability. These probabilities are dictated by the Boltzmann distribution, linking the likelihood of the system occupying a specific state to its energy and temperature. By executing a large number of Monte Carlo steps, the system's statistical properties can be reliably estimated. In radmc3D, the Monte Carlo method, originally proposed by Bjorkman Wood (2001, ApJ 554, 615), augmented with enhancements such as the continuous absorption technique introduced by Lucy (1999, AA 344, 282), is employed to compute dust temperatures.

3.4.3 Bjorkman Wood Algorithm (2001)

The core concept of the Bjorkman Wood algorithm revolves around treating each absorption re-emission event akin to a scattering event, albeit with alterations in both angle and frequency. The algorithm operates by accumulating energy within each cell, facilitating the computation of the source function, which, in this context, pertains to the dust temperature. While scattering events maintain frequency but alter angle, absorption and re-emission events induce changes in both angle and frequency. This approach allows for a comprehensive modeling of radiative transfer processes, essential for accurately determining dust temperatures within astrophysical environments.

Advantages

1. This method gives excellent luminosity conservation.
2. No convergence checking is needed

3. And is extremely stable.

Disadvantages

1. The photons might get stuck in ultra high regions
2. This method does not work for temperature-dependent K_v

3.4.4 How does the method work?

The following steps are followed while executing a Thermal Monte Carlo simulation:

1. The first step is to identify a source of luminosity. These could be stars, continuum stellar source or viscous heating/internal heating of dust.
2. This method does not work for temperature dependent K_v
3. To compute the dust temperature we must have atleast one source of luminosity, else the equilibrium dust temperature would be 0 everywhere.
4. Next the total luminosity is divided using a parameter ‘nphot’ that is used to control the number of photon packages used in the Monte Carlo radiative transfer calculations. It is set to 100,000 by default but can be set to any value by the user.
5. These sources then release photon packages one at a time. Photon packages can bounce off dust particles, collect energy, and then reemit it in a different direction and at a different wavelength. According to Bjorkman Wood’s recipe (2001, ApJ 554, 615) the wavelength is selected.
6. We increase the dust’s temperature whenever a photon bundle reaches a cell, whereas Bjorkman Wood only do so after a discrete absorption event has occurred.

7. Until it leaves the model through the exterior edge of the grid, which for cartesian coordinates is any of the grid edges in x, y, or z, and for spherical coordinates is the outer edge of r, each photon packet will bounce around the model and never get lost.
8. A fresh photon package is launched after it escapes until it too escapes. The dust temperature that is still present after all photon packages have been launched and ejected serves as the definitive determination of the dust temperature.
9. It has been estimated what the equilibrium dust temperature is. It is assumed that each dust particle absorbs the same amount of energy as it emits. Given that the heating and cooling times for dust grains are often quite brief relative to any time dependent dynamics of the system, this approximation is probably very accurate in the majority of circumstances. However, there are other circumstances in which this might not be the case, such as when gas is compressed quickly, close to shock waves, or in extremely optically thick places.

3.5 Modified Random Walk Method

In Thermal Monte Carlo simulations, the persistent retention of photon packages within the system until their exit can lead to pronounced computational inefficiencies in highly optically thick models. This inefficiency is primarily attributable to the propensity of photon packages to become ensnared within dense regions, thereby instigating an excessive number of absorption+re-emission or scattering events, often reaching magnitudes in the millions or billions. Furthermore, the attainment of dependable temperatures within such regions necessitates a considerable allocation of photon packages, exacerbating the deceleration of simulations. To circumvent these challenges, the Modified Random Walk technique is adopted. This technique independently ascertains the probability of scattering and absorption for each infinitesimal segment along a photon's trajectory, thereby affording a more refined depiction of photon-medium interactions, particularly in scenarios characterized by substantial optical depth.

Chapter 4

Methodology

In this section, we present our numerical framework and the various methods used to calculate the radiative transfer in our model. To prepare the inputs for the stars.inp input file, we needed the co-ordinates, mass, radius, temperature and luminosity of the stars. Use the relation:

$$distance(d) = \frac{1000}{parallax}$$

To get the distance of the star from the sun and then used the following transformation to get the cartesian co-ordinates :

$$\begin{aligned}x &= Distance * \cos b * \cos l \\y &= Distance * \cos b * \sin l \\z &= Distance * \sin b\end{aligned}$$

Where l and b are galactic co-ordinates in terms of longitude and latitude.

4.1 Model Setup

4.1.1 One Star Model

Prior to modelling, the initial stage of our study involves configuring the model setup to accurately represent a one star system whose emission peaks at NIR. For this, we consider stars with the necessary luminosity, mass, and size. The problem setup.py file is utilized to define the parameters and specifications of the model. We build upon the *run_simple1*; a gaussian model, example provided in the radmc3d code repository, we incorporate a Henyey-Greenstein function with scattering mode = 2 to account for the complex scattering behavior observed in the Taurus-Perseus, L183, Cepheus and Chameleon region. This choice enables a more realistic approximation of the scattering processes. The model is of a one star system

and the interstellar dust is considered as a blob with a radius of 10AU and dust density of $20e-16\text{g/cm}^3$. The problem setup code is defined below:

```
1  #
2  # Import NumPy for array handling
3  #
4  import numpy as np
5  #
6  # Import plotting libraries (start Python with ipython --
7  #   matplotlib)
8  #
9  #from mpl_toolkits.mplot3d import axes3d
10 #from matplotlib import pyplot as plt
11 #
12 # Some natural constants
13 #
14 au    = 1.49598e13      # Astronomical Unit          [cm]
15 pc    = 3.08572e18      # Parsec                      [cm]
16 ms    = 1.98892e33      # Solar mass                  [g]
17 ts    = 5.78e3           # Solar temperature            [K]
18 ls    = 3.8525e33        # Solar luminosity             [erg/s]
19 rs    = 6.96e10          # Solar radius                 [cm]
20 #
21 # Monte Carlo parameters
22 nphot = 1000000
23 #
24 # Grid parameters
25 #
26 nx    = 32
27 ny    = 32
28 nz    = 32
29 sizex = 14*au
30 sizey = 14*au
31 sizez = 14*au
32 #
33 # Model parameters
34 #
35 radius = 10*au
36 rho0   = 12*1e-16
37 #
38 # Star parameters
39 #
40 mstar  = 2*ms
```

```

41 rstar      = 12*rs
42 tstar      = 0.20*ts
43 pstar      = np.array([0.,0.,0.])
44 #
45 # Make the coordinates
46 #
47 xi         = np.linspace(-sizex,sizex,nx+1)
48 yi         = np.linspace(-sizey,sizey,ny+1)
49 zi         = np.linspace(-sizez,sizez,nz+1)
50 xc         = 0.5 * ( xi[0:nx] + xi[1:nx+1] )
51 yc         = 0.5 * ( yi[0:ny] + yi[1:ny+1] )
52 zc         = 0.5 * ( zi[0:nz] + zi[1:nz+1] )
53 #
54 # Make the dust density model
55 #
56 qq         = np.meshgrid(xc,yc,zc,indexing='ij')
57 xx         = qq[0]
58 yy         = qq[1]
59 zz         = qq[2]
60 rr         = np.sqrt(xx**2+yy**2+zz**2)
61 rhod       = rho0 * np.exp(-(rr**2/radius**2)/2.0)
62 #
63 # Write the wavelength_micron.inp file
64 #
65 lam1       = 0.1e0
66 lam2       = 7.0e0
67 lam3       = 25.e0
68 lam4       = 1.0e4
69 n12        = 20
70 n23        = 100
71 n34        = 30
72 lam12      = np.logspace(np.log10(lam1),np.log10(lam2),n12,
    endpoint=False)
73 lam23      = np.logspace(np.log10(lam2),np.log10(lam3),n23,
    endpoint=False)
74 lam34      = np.logspace(np.log10(lam3),np.log10(lam4),n34,
    endpoint=True)
75 lam         = np.concatenate([lam12, lam23, lam34])
76 nlam        = lam.size
77 #
78 # Write the wavelength file
79 #
80 with open('wavelength_micron.inp','w+') as f:
81     f.write('%d\n'%(nlam))
82     for value in lam:

```

```

83         f.write('%13.6e\n' % (value))
84 #
85 #
86 # Write the stars.inp file
87 #
88 with open('stars.inp', 'w+') as f:
89     f.write('2\n')
90     f.write('1 %d\n\n' % (nlam))
91     f.write('%13.6e %13.6e %13.6e %13.6e %13.6e\n\n' % (rstar,
92     mstar, pstar[0], pstar[1], pstar[2]))
93     for value in lam:
94         f.write('%13.6e\n' % (value))
95     f.write('\n%13.6e\n' % (-tstar))
96 #
97 # Write the grid file
98 #
99 with open('amr_grid.inp', 'w+') as f:
100     f.write('1\n')                                # iformat
101     f.write('0\n')                                # AMR grid style (0=
102     regular grid, no AMR)
103     f.write('0\n')                                # Coordinate system
104     f.write('0\n')                                # gridinfo
105     f.write('1 1 1\n')                            # Include x,y,z
106     coordinate
107     f.write('%d %d %d\n' % (nx, ny, nz))        # Size of grid
108     for value in xi:
109         f.write('%13.6e\n' % (value))            # X coordinates (cell
110     walls)
111     for value in yi:
112         f.write('%13.6e\n' % (value))            # Y coordinates (cell
113     walls)
114     for value in zi:
115         f.write('%13.6e\n' % (value))            # Z coordinates (cell
116     walls)
117 #
118 # Write the density file
119 #
120 with open('dust_density.inp', 'w+') as f:
121     f.write('1\n')                                # Format number
122     f.write('%d\n' % (nx*ny*nz))                # Nr of cells
123     f.write('1\n')                                # Nr of dust species
124     data = rhod.ravel(order='F')                 # Create a 1-D view,
125     fortran-style indexing
126     data.tofile(f, sep='\n', format="%13.6e")
127     f.write('\n')

```

```

121 #
122 # Dust opacity control file
123 #
124 with open('dustopac.inp','w+') as f:
125     f.write('2          Format number of this file\n')
126     f.write('1          Nr of dust species\n')
127     f.write('
=====
128     f.write('1          Way in which this dust species is
129     f.write('0          0=Thermal grain\n')
130     f.write('silicate      Extension of name of dustkappa_
131     ***.inp file\n')
132     f.write('
-----
133     f.write('n')
134 #
135 # Write the radmc3d.inp control file
136 #
137 with open('radmc3d.inp','w+') as f:
138     f.write('nphot = %d\n'%(nphot))
139     f.write('scattering_mode_max = 2\n')    # Put this to 1 for
140     f.write('isotropic scattering
141     f.write('iranfreqmode = 1\n')


```

To run a Monte Carlo simulation, run the following code

```

1      radmc3d mctherm
2


```

Now for scattering, run the following code

```

1      radmc3d sed
2


```

We plot the image, SED and the temporal distribution by defining another file problem plot.py. It is defined as follows:

```

1 #
2 import problem_setup as p
3 import numpy as np
4 from mpl_toolkits.mplot3d import axes3d


```

```

5 from matplotlib import pyplot as plt
6 from matplotlib import cm
7 from radmc3dPy.image import *
8 from radmc3dPy.analyze import *
9
10 #
11 # View a 2-D slice of the 3-D array of the setup
12 #
13 xx = p.xx[:, :, 16]
14 yy = p.yy[:, :, 16]
15 data = p.rhod[:, :, 16]
16 fig1 = plt.figure()
17 ax = fig1.add_subplot(projection='3d')
18 #ax.plot_wireframe(xx, yy, data, rstride=1, cstride=1)
19 ax.plot_surface(xx, yy, data, rstride=1, cstride=1, cmap=cm.
    coolwarm, linewidth=0, antialiased=False)
20
21 #
22 # Plot the opacity table
23 #
24 o = readOpac(ext='silicate')
25 plt.figure()
26 plt.loglog(o.wav[0], o.kabs[0], label=r'$\kappa_{\nu}^{\mathrm{abs}}$ (absorption)')
27 plt.loglog(o.wav[0], o.ksca[0], ':', label=r'$\kappa_{\nu}^{\mathrm{scat}}$ (scattering)')
28 plt.ylim((1e-2, 1e5))
29 plt.xlabel(r'$\lambda; [\mu\mathrm{m}]$')
30 plt.ylabel(r'$\kappa_{\nu}; [\mathrm{cm}^2/\mathrm{g}]$')
31 plt.title(r'Dust opacity (olivine, $a=0.1\mu\mathrm{m}$)')
32 plt.legend()
33
34 #
35 # Make and plot an example image
36 #
37 makeImage(npix=50, incl=60., phi=30., wav=3.6, sizeau=45)      # This
    calls radmc3d
38 fig2 = plt.figure()
39 a=readImage()
40 plotImage(a, log=True, au=True, maxlog=6, cmap='hot')
41
42 #
43 # Make the SED, by calling RADMC-3D
44 #
45 os.system("radmc3d sed incl 60 phi 30")

```

```

46
47 #
48 # Plotting it "by hand", the SED as seen at 1 pc distance
49 #
50 fig3 = plt.figure()
51 s = readSpectrum()
52 lam = s[:,0]
53 nu = 1e4*cc/lam
54 fnu = s[:,1]
55 nufnu = nu*fnu
56 plt.plot(lam,nufnu)
57 plt.xscale('log')
58 plt.yscale('log')
59 plt.axis([1e-1, 1e4, 1e-10, 1e-4])
60 plt.xlabel('$\lambda; [\mu \mathrm{m}]$')
61 plt.ylabel('$\nu F_\nu; [\mathrm{erg}/\mathrm{cm}^2\mathrm{s}]$')
62 #
63 #
64 # Use the radmc3dPy.analyze tool set for plotting the SED,
65 # this time let's plot nuLnu in units of Lsun
66 #
67 fig4 = plt.figure()
68 plotSpectrum(s,nulnu=True,lsun=True,xlg=True,ylg=False,micron=
    True)
69 plt.axis([1e-1,1e4,1e-8,1])
70
71 #
72 # Use the radmc3dPy.analyze tool set to read in the dust
    temperatures
73 # calculated by the command-line command "radmc3d mctherm"
74 #
75 q = readData()
76 fig5 = plt.figure()
77 ay = fig5.add_subplot(projection='3d')
78 qq = np.meshgrid(q.grid.x,q.grid.y,q.grid.z,indexing='ij')
79 xx = qq[0][:,:,16]
80 yy = qq[1][:,:,16]
81 dd = q.dusttemp[:,:,:16,0] # The extra "0" is because of
    possible multiple dust species; here only 1 dust species
82 ay.plot_surface(xx, yy, dd, rstride=1, cstride=1, cmap=cm.
    coolwarm, linewidth=1)
83
84
85 plt.show()

```

problem plot.py

The results of the simulation are discussed in the next Chapter.

4.2 Verifying the results

After getting the required plots from our model, we have to compare our results with coreshine observations, specifically the intensity at $3.6\mu\text{m}$. We used an Astronomical Imaging and Visualization tool SAOImage DS9 to process the image outputted by our model to compare the NIR intensities at various locations and get the average to have a fair idea about the mean intensity of the system as compared to coreshine observations.

Chapter 5

Results and Discussion

5.1 Coreshine Data

The Table for the coreshine intensity is at page 35 and 36.

5.2 One Star system

We obtained the SED as in 6.1 and 6.2, we see a distinctive dip near $10\mu\text{m}$ wavelength, which might be due to the presence of Polycyclic Aromatic Hydrocarbons (PAHs) which are the primary source of absorption medium in lower wavelengths.

5.2.1 For Isotropic Scattering

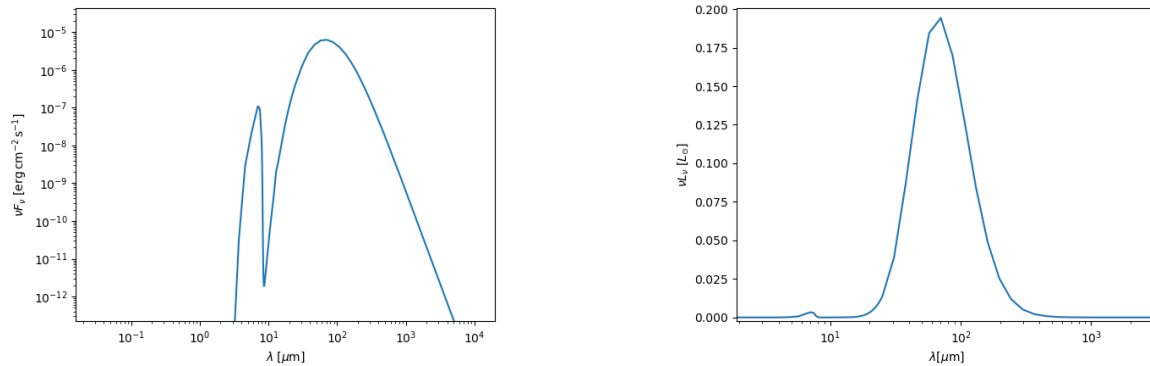


Fig 6.1 Left: SED; Right : Relative Brightness

5.3 For Anisotropic Scattering

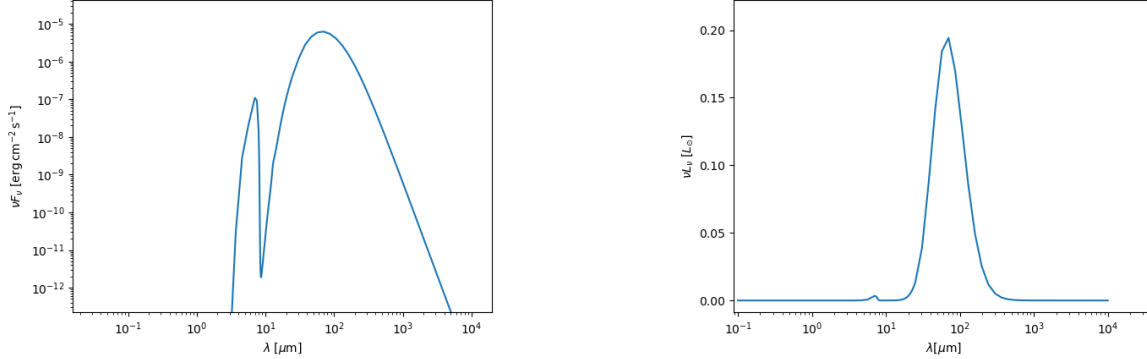


Fig 6.2 Left: SED; Right : Relative Brightness

5.3.1 For Userdefined Crossection and Phase Function Scattering

Grain size = 3.20000; Wavelength = 3.6000; Extinction Opacity = 1.399E+00;
 Absorption Opacity= 4.549E-01; Scattering opacity = 9.439E-01; Phase
 functions: e = 1.257E-06; f = 1.519E-06; g = 8.120E-01

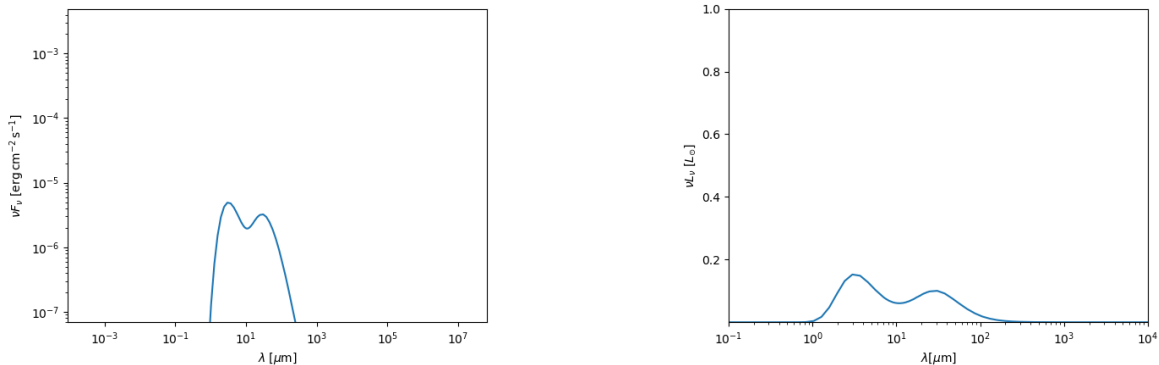


Fig 6.2 Left: SED; Right : Relative Brightness

5.3.2 Model Images

From our simulations, we have obtained the following results. 6.3 are an images of the system, while the left is from isotropic scattering and right from anisotropic scattering and 6.4 is for user defined scattering and phase functions. The image is modelled at a wavelenngth, λ of $3.6\mu\text{m}$. The X and Y axis represent the spatial axes while the colour bar represents the intensity of the star at a wavelength of $3.6\mu\text{m}$ to the maximum intensity at that wavelength. Since the maximum intensity occurs at the star centers we can see that those are the brightest areas while it decreases progressively. Figure 6.5 represents the Extinction curve or the extinction cross-section for (Isotropic and Anisotropic) as a function of wavelength plot for the system assuming the grain size to be $3.2 \mu\text{m}$. It is a measure of how a photon will be scattered by a dust grain We observe that the dust opacity or absoption of light scatv and absv is quite high for wavelengths $10 \mu\text{m}$ and $18 \mu\text{m}$. This can be attributed to the presence of Silicates which show characteristic absorption at those wavelengths.

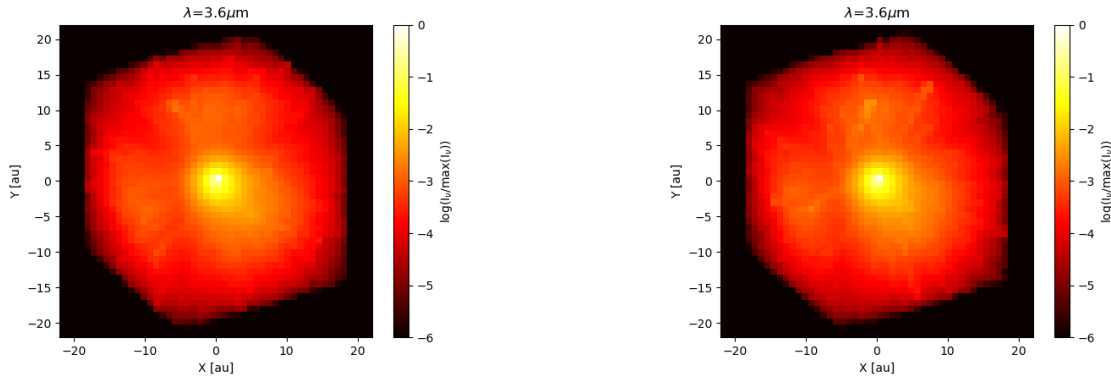


Fig 6.3 Left: Isotropic Scattering; Right : Anisotropic Scattering

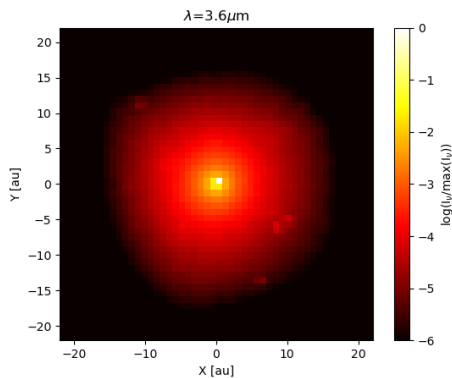


Fig 6.4 Image for user defined scattering

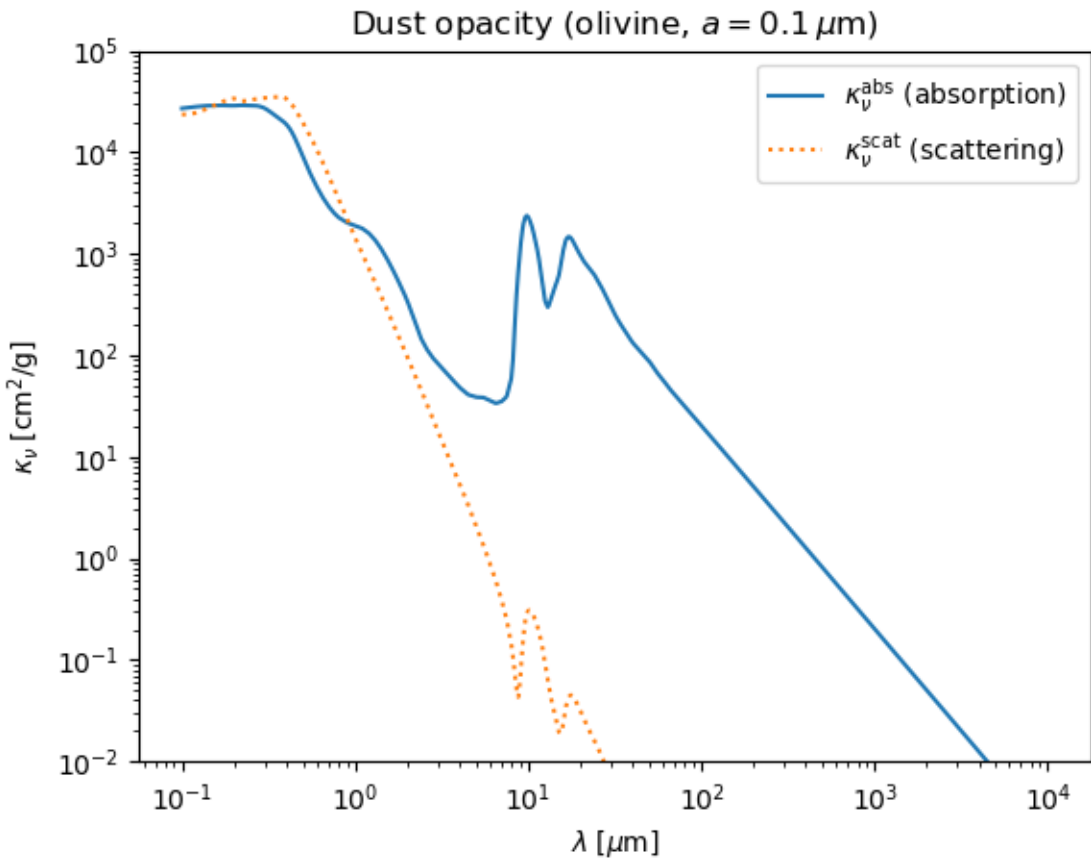
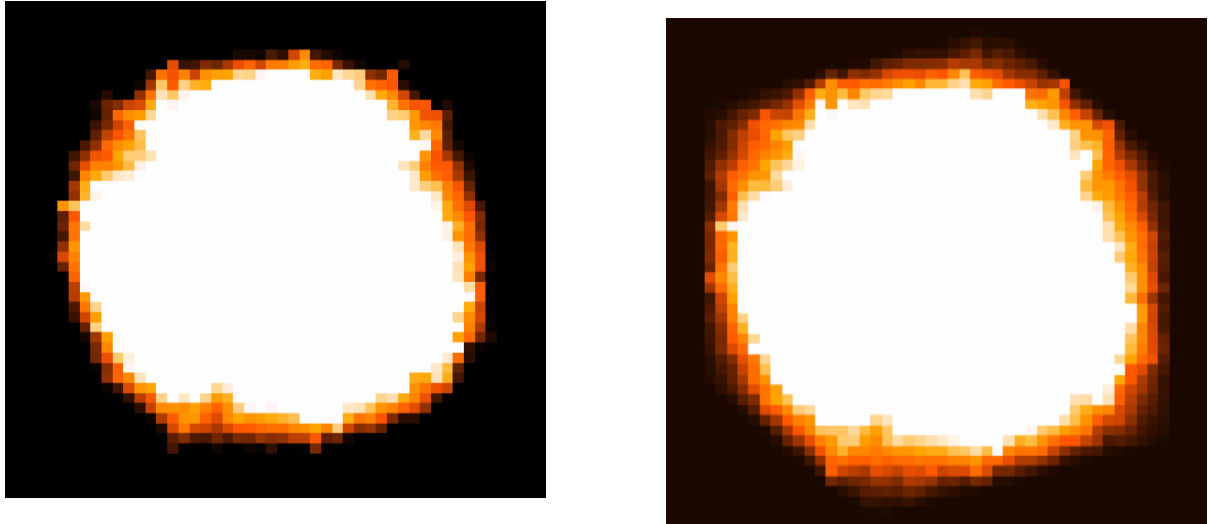


Fig 6.5 Extinction curves(a function of wavelength)

5.4 Post-processing and comparision with real-world observations

On further processing the image shown in Figure 6.3 with the SAOImage DS9 software, we made adjustments to the scale. The resulting image is depicted in Figure 6.5. The image obtained from DS9 has a mean intensity value of $555.98 \text{ KJy } sr^{-1}$ for isotropic scattering and $682.29 \text{ KJy } sr^{-1}$ for anisotropic scattering. In comparison, for our model, the coreshine observational range at $3.6\mu\text{m}$ is given in table. The observation of core-shine ranges from $10-390 \text{ KJy } sr^{-1}$. When averaging this intensities, we observe that they align with the order of magnitude of the intensities with the coreshine observation. However, determining the exact values for the intensities, both for the model and the coreshine, would require further computation, which has been left as a scope for future work.



Left : Isotropic Scattering; Right : Anisotropic Scattering

Chapter 6

Conclusion and Future Work

In this report, we have focused on modeling the dust in the regions, having a star in the Taurus-Perseus, L183, Chameleon and Cepheus. Our objective was to obtain the system's image and spectral energy distributions (SEDs) to gain insights into the characteristics of interstellar scattering in the region and also compare the IR scattering intensity to coreshine observations. During our analysis, we found that the majority of the extinction in the system can be attributed to polycyclic aromatic hydrocarbons (PAHs) and Silicates. Notably, we observed distinct absorptions occurring at approximately $10\mu\text{m}$, particularly when considering a grain size of $3.2\ \mu\text{m}$ which was caused due to the presence of Silicates. We also found that the scattering intensity of our model is quite in agreement with coreshine observations.

6.1 Future Work

While our initial findings provide valuable insights, further investigation and fine-tuning of our model necessary to model the extinction accurately. In the future, we intend to model region by region of the molecular dust to get a better picture of the extinction that occurs in these regions. By examining these graphs and values at NIR alongside coreshine data, we can ascertain the reliability and accuracy of our model, ultimately contributing to a deeper understanding of interstellar phenomena, in the Taurus-Perseus, L183, Chameleon, Cepheus regions.

| Taurus-Perseus | | |
|------------------------|-----------------------------------------|---------------------------|
| Name | 3.6 m intensity (kJy sr ⁻¹) | Protostar |
| G171.80-09.78 | 10 | |
| CB24 | 15 | |
| L1503 | 22 | |
| G179.18-19.62 | 22 | |
| G182.19-17.71 | 23 | |
| G170.81-18.34 | 26 | |
| L1552 | 26 | |
| G169.82-19.39 | 27 | |
| CB20 | 27 | |
| G173.45-13.34 | 30 | |
| G177.89-20.16 | 33 | |
| B18-3 = G174.39-13.43 | 35 | |
| G154.68-15.34 | 49 | |
| G170.99-15.81 | 36 | |
| L1506C | 33 | |
| L1507A (G171.51-10.59) | 41 | |
| IRAS 03282+3035 | 47 | IRAS 03282+3035 |
| G173.69-15.55 | 32 | |
| L1544 | 39 | |
| L1512 | 30 | |
| L1521E | 51 | |
| L1498 | 34 | |
| G171.34-10.67 | 58 | |
| G170.26-16.02 | 87 | IRAS 04181+2654AB |
| L1521F | 53 | VeLLO |
| L1517A | 57 | |
| L1517B | 43 | |
| G157.10-08.70 | 34 | IRAS 03586+4112 (?)d |
| L1517C | 29 | |
| L1507 | 41 | 2MASS J04432023+2940060 |
| IRAM04191 | 140 | IRAM04191-IRS |
| L1439 | 81 | IRAS 04559+5200 |
| TMC2 | 100 | IRAS 04294+2413 |
| L1448mm | 59 | L1448-mm |
| G163.21-08.40 | 67 | IRAS 04218+3708 (?)d |
| G157.12-11.56 | 390 | IRAS 03484+3845 (?)d |
| G155.45-14.59 | 210 | IRAS 03330+3727 (?)d |
| G160.51-16.84 | 61 | B5 IRS1 (IRAS 03445+3242) |
| G171.91-15.65 | 310 | DG Tau B |
| Barnard18-1 | 97 | IRAS 04292+2422(E+W) |
| G163.32-08.42 | 63 | IRAS 04223+3700 |
| G158.86-21.60 | 74 | IRAS 03249+2957 |
| Barnard | 100 | IRAS 03301+3057 (cluster) |
| L183 | 58 | |
| L134 | >30 | 35 |

Combined table for Taurus-Perseus, Chameleon, and Cepheus

| Chameleon | | |
|---------------|-----------------------------------------|---------------------------|
| Name | 3.6 m intensity (kJy sr ⁻¹) | Protostar |
| G302.89-14.05 | 16 | |
| G298.34-13.03 | 25 | |
| G303.28-13.32 | 25 | |
| Mu8 | 27 | |
| G297.09-16.02 | 39 | |
| G303.09-16.04 | 77 | |
| G303.68-15.32 | 21 | |
| G303.39-14.26 | 150 | IRAS 12553-7651 |
| G303.15-17.34 | 32 | |
| G303.72-14.86 | 100 | IRAS 13014-7723 |
| Cepheus | | |
| Name | 3.6 m intensity (kJy sr ⁻¹) | Protostar |
| G093.20+09.53 | 18 | |
| L1155E | 22 | |
| G093.16+09.61 | 24 | |
| G130.56+11.51 | 24 | |
| L1157 | 28 | IRAS 20386+6751 |
| L1155C | 29 | |
| L1247 | 110 | |
| L1251A | 62 | L1251A-IRS1-4 |
| L1333" | 25 | |
| L1148 | 24 | L1148-IRS |
| L1152 | 39 | L1152 1-3 |
| L1262 | 92 | IRAS 23238+7401 |
| L1157-outflow | 31 | Outflow shock region ? |
| L1228 | 110 | IRAS 20582+7724 (cluster) |
| L1221 | 160 | L1221-IRSI & 3 |
| L1251C | 260 | IRAS 22343+7501 (cluster) |
| L1251B | 160 | IRAS 22376+7455 (cluster) |

Combined table for Taurus-Perseus, Chameleon, and Cepheus (Part 2)
[12]

References

- [1] F. H. Shu, F. C. Adams, and S. Lizano, “Star formation in molecular clouds: Observation and theory,” *Annual Review of Astronomy and Astrophysics*, vol. 25, no. 1, pp. 23–81, 1987.
- [2] J. Williams, L. Blitz, and C. McKee, “The structure and evolution of molecular clouds: from clumps to cores to the imf,” March 1999.
- [3] C. J. Lada, E. A. Lada, D. P. Clemens, and J. Bally, *Mapping Dust Extinction with IR Cameras*, pp. 473–480. Dordrecht: Springer Netherlands, 1994.
- [4] D. A. Ostlie and B. W. Carroll, *An introduction to modern astrophysics*. Addison Wesley Reading, MA, USA, 2007.
- [5] R. B. Larson, “Numerical calculations of the dynamics of a collapsing proto-star,” *Monthly Notices of the Royal Astronomical Society*, vol. 145, no. 3, pp. 271–295, 1969.
- [6] S. W. Stahler and F. Palla, *The formation of stars*. John Wiley & Sons, 2008.
- [7] J. M. Scalo, “The Stellar Initial Mass Function,” 1998.
- [8] G. Dopcke, S. C. Glover, P. C. Clark, and R. S. Klessen, “The effect of dust cooling on low-metallicity star-forming clouds,” *The Astrophysical Journal Letters*, vol. 729, no. 1, p. L3, 2011.
- [9] I. Pascucci, D. Apai, K. Luhman, T. Henning, J. Bouwman, M. Meyer, F. Lahuis, and A. Natta, “The different evolution of gas and dust in disks around sun-like and cool stars,” *The Astrophysical Journal*, vol. 696, no. 1, p. 143, 2009.
- [10] W.-R. H. A. S. A. L. H. T. M. Steinke, L. M. Oskinova, “Analysis of the WN star WR 102c, its WR nebula, and the associated cluster of massive stars in the Sickle Nebula,” 2016.
- [11] B. Draine, “Scattering by interstellar dust grains. i. optical and ultraviolet,” *Astrophysical Journal*, vol. 598, April 2003.

- [12] Lefèvre, C., Pagani, L., Juvela, M., Paladini, R., Lallement, R., Marshall, D. J., Andersen, M., Bacmann, A., McGehee, P. M., Montier, L., Noriega-Crespo, A., Pelkonen, V.-M., Ristorcelli, I., Steinacker, J. (Year). "Dust properties inside molecular clouds from coreshine modeling and observations." *Astronomy and Astrophysics*.
- [13] Smithsonian Astrophysical Observatory, "SAOImage DS9." <https://sites.google.com/cfa.harvard.edu/saoimageds9>,
- [14] Henyey, L. G., Greenstein, J. L. (1941). Diffuse radiation in the galaxy. *The Astrophysical Journal*, 93, 70.